

Persisting of the Lone-Pair-Driven Polar Distortion with Electron Doping

Xu He¹ and Kui-juan Jin^{1,2,*}

¹Beijing National Laboratory for Condensed Matter Physics,
Institute of Physics, Chinese Academy of Sciences, Beijing 100190, China
²Collaborative Innovation Center of Quantum Matter, Beijing 100190, China

“Ferroelectric” metals have attracted great interests since the recent identification of the broken inversion symmetry in the metallic perovskite LiOsO₃. Free electrons can screen out long range Coulomb interaction and destroy the polar distortion in some ferroelectric materials, whereas polar distortion and metallicity coexist in “ferroelectric” metals. So the problem is how to ensure that the polar distortion is not destroyed by the screening effect? In this work, by studying the change of polar distortion with electron doping in the lone-pair-driven ferroelectric material PbTiO₃, we found that the screening effect doesn’t strongly affect the formation of the electron long pairs, because the energy range of the electron states related to the lone pair is far away from the Fermi energy in PbTiO₃. The lone-pair-driven polar distortion not only persists, but also gets enhanced with electron doping in PbTiO₃, which is a combined effect of the lone pair and the increasing of the lattice volume caused by the electron doping. These results show that the existing of long-pair-stereoactive ions in the metallic perovskite can be one warrantable way to keep or even enhance the polar distortion by electron doping in spite of the screening effect, which strongly suggests that the lone-pair-stereoactive ions can be used in designing “ferroelectric” metals.

PACS numbers: 77.80.-e, 77.84.Ek

I. INTRODUCTION

Free carriers are harmful for polar distortion in many cases. For example, in a prototypical ferroelectric material BaTiO₃, the ferroelectric distortion is weakened with electron doping, and eventually disappears when a critical concentration is reached¹⁻⁴. The screening of the Coulomb interaction was believed to be the reason for the weakening or disappearing of the polar distortion for BaTiO₃^{3,4}. Although the screening effect of the carriers can inhibit the polar distortion also for many other ferroelectric materials, there are exceptions which have attracted a lot of attentions and efforts. Anderson and Blount pointed out that while free electrons can screen out the electric field, the transverse optical soft phonons can lead to polar distortion⁵. A few “ferroelectric” metals, or more precisely non-central-symmetric metals (NCSMs) have been found, such as perovskite structure LiOsO₃⁷. In LiOsO₃, the ferroelectricity is due to the Li-O displacement, whereas the Fermi level lies in the Os bands⁹⁻¹². Xiang suggested that the long range Coulomb interaction is not necessary for the polar distortion; the short-range pair interactions, which are not screened out by free electrons, can drive the polar distortion¹⁰. Puggioni and Rondinelli proposed that the non-centrosymmetric structure can exist if the coupling of the soft phonon mode and the electrons at the Fermi level is weak⁶. Benedek and Birol proposed that polar distortion can emerge through a geometric mechanism in metals⁸.

Although the NCSM structures are no longer suitable for the usage as ferroelectric materials because of the metallicity, other interesting properties are found in NCSMs, like the unconventional optical responses^{13,14}, magnetoelectricity¹⁵, superconductivity¹⁶, and thermoelectricity⁶. A deeper under-

standing of the mechanisms of NCSM could help finding new NCSMs. The purpose of this work is to seek a possible mechanism of NCSMs so new NCSMs can be found or designed.

In this work, we show that the lone-pair-driven polar distortion is compatible with metallicity. The polar distortion can even be enhanced with the increasing of the free electron concentration in some materials. In the lone-pair-driven ferroelectric materials, the electronic states related to the lone pairs are often not at the Fermi energies. Thus the coupling between the electronic states at the Fermi energy and the soft phonons driven by the lone pairs may be weak. Consequently, the ferroelectric distortion may persist with the carrier doping. We firstly show that the polar distortion in PbTiO₃ not only survives the the screening effect, but also is enhanced with the electron doping. Then by analyzing the evolution of the phonon and electronic structures with electron doping, we’ll show why the polar distortion driven by the electron lone pair is not strongly coupled to the electron doping. Thirdly, we’ll show that enhancement of the polar distortion is a combined effect of the lone pair and the increasing of the lattice volume caused by the electron doping. Lastly, we discuss the generalizability of the results from PbTiO₃ to other lone-pair-driven ferroelectric materials and propose that the lone-pair stereoactive ions can be used for the designing of NCSMs.

II. METHODS

The density functional theory (DFT) calculations were carried out by using the projected augmented wave (PAW)¹⁷ pseudopotentials as implemented in the Vienna *ab initio* simulation package (VASP)¹⁸. The energy cutoff of the plane wave basis set was 500 eV. The exchange correlation functional with local density approximation (LDA) as parameterized by Perdew and Zunger (PZ)¹⁹ was used. The reference electronic configurations for the pseudopotentials are Pb 5d¹⁰6s²6p², Ti

* Correspondence and requests for materials should be addressed to Kui-juan Jin. Email: kjjin@iphy.ac.cn

$3s^23p^63d^4$, and O $2s^22p^6$, respectively. An $8 \times 8 \times 8$ Γ -centered k -point mesh was used to represent the reciprocal space. The calculated $P4mm$ structure has a tetragonality (c/a) of 1.04 and a volume of 60.2 \AA^3 , agreeing well with the experimental data and previous DFT calculations^{20,21}.

For the calculations of the structures with electron doping, the image charge correction²² and the potential-alignment correction²³ were used. The phonon frequencies were calculated using the density functional perturbation theory²⁴ (DFPT) method as implemented in VASP and the phonopy²⁵ package. A $2 \times 2 \times 2$ supercell of 40 atoms was used for the phonon calculation. The phonon frequencies were calculated with the structures fully relaxed. A Γ -centered $20 \times 20 \times 20$ Monkhorst-Pack grid was used to calculate the phonon density of states (PDOS). The longitudinal-optical-transverse-optical (LO-TO) splitting was not considered due to the existence of the free charges. The crystal orbital hamilton population^{26,27} (COHP) analyses were carried out with the LOBSTER²⁸ code. The contour maps of the electron localization functions²⁹ (ELFs) were visualized using the VESTA package³⁰ to show the electron lone pairs. The crystal structures were also visualized using the VESTA package.

The ferroelectric polarization in a structure with free charges is not well defined. Therefore, the structural polar distortion is discussed in the present work instead of the ferroelectric polarization.

III. RESULTS AND DISCUSSION

Firstly, we show the enhancement of the polar distortion with electron doping in PbTiO_3 . The change of the $P4mm$ PbTiO_3 structure with the concentration of the doped carriers is shown in Fig. 1. As the concentration of the doped electrons increases, the tetragonality (c/a) of the lattice increases, as shown in Fig. 1 (a); the relative displacements of the Pb and Ti cations from the O anions increase, as shown in Fig. 1 (b). These phenomena show the enhancement of the polar distortion, in contrast to what happens in the $P4mm$ BaTiO_3 .¹⁻⁴

In BaTiO_3 , the decreasing of the polar distortion with electron doping is because of the screening effect^{3,4}. The doped electrons screen out the long range Coulomb interaction. The screening length λ can be estimated with the Thomas-Fermi model $\lambda = \sqrt{\epsilon/e^2D(E_F)}$, where ϵ is the dielectric permittivity, and $D(E_F)$ is the density of states (DOS) at the Fermi level. As the concentration of doped electrons increases, the DOS at the Fermi energy increases, and thus the screening length decreases. The values of ϵ and the values of $D(E_F)$ for PbTiO_3 are close to those for BaTiO_3 , respectively. ($\epsilon(\text{PbTiO}_3)$ and $\epsilon(\text{BaTiO}_3)$ are $81\epsilon_0$ and $78\epsilon_0$ from the LDA and DFPT³¹ calculation³², respectively. When the concentration of electrons is 0.2 e/u.c. , the $D(E_F)$ are 0.7 and $1.1 \text{ states/(eV}\cdot\text{u.c.)}$, and consequently the screening length are about 5 \AA and 6 \AA in PbTiO_3 and BaTiO_3 , respectively.) Therefore, the screening effects of the long-range Coulomb interaction are comparable in these two materials. The polar distortion is gradually destroyed by the screening effect in BaTiO_3 . Then what is the intrinsic reason for the opposite

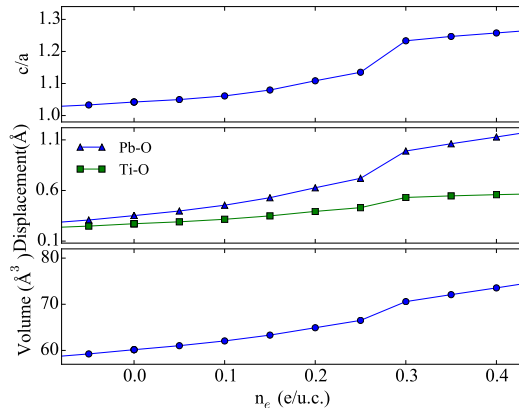


FIG. 1: (a) The ratio of out-of-plane lattice constant c and the in-plane lattice constant a , (b) relative displacements of Pb-O and Ti-O, and (c) volume as functions of doped electron density n_e .

trend of the polar distortion with doped electrons in PbTiO_3 from that in BaTiO_3 ?

The mechanisms of the ferroelectricity in PbTiO_3 and BaTiO_3 are different. In the ABO_3 ferroelectric perovskite structures, the tolerance factor t , defined as $t = \frac{r_A+r_O}{\sqrt{2}(r_B+r_O)}$, is a quantity related to the distortion. t larger than 1 indicates that the B-O bonds are stretched, so that the B-site ion in an O-B-O chain displaces towards an O ion (eg. in BaTiO_3); whereas t smaller than 1 indicates the A-site polar instability (eg. in LiOsO_3 ¹⁰). The decrease of t is a reason for the reduction of the ferroelectric distortion with electron doping in BaTiO_3 ⁴, because the doped electrons mainly stay on the Ti sites, increasing the sizes of Ti ions and decreasing t . In PbTiO_3 , the Shannon ionic radii of Pb, Ti, and O are 1.63 \AA , 0.56 \AA , and 1.21 \AA , respectively³³. Thus t is about 1.02, slightly larger than 1. However, since the electron distribution of the Pb ion is highly asymmetric in the $P4mm$ PbTiO_3 due to the Pb lone pair, the ionic radii are not good quantities for describing the Pb-O bond length any more. The polar distortion in PbTiO_3 is simply driven by the Ti site instability, but the Pb site plays a crucial rule in the polar distortion of PbTiO_3 . Due to the anisotropic distribution of the lone pair electrons, the Pb ionic radius becomes asymmetric, which drives the Pb ions away from their central symmetric positions.

To see which site is responsible for the polar distortion and how the polar instability couples with the electron doping, we consider the evolution of the phonon modes in the paraelectric $Pm\bar{3}m$ phase and those in the ferroelectric $P4mm$ phase with the electron doping. The transition to a ferroelectric phase from a paraelectric phase is featured with imaginary phonon frequencies in the paraelectric phase. The phonon bands of both $Pm\bar{3}m$ phase and $P4mm$ phase were calculated, as shown in Fig. 2. Without electron doping, the imaginary frequencies are at Γ , R , and M in the $Pm\bar{3}m$ phase, as shown in Fig. 2 (a). With electrons doped, the imaginary frequency at Γ point (Fig. 2 (b)) corresponding to the ferroelectric distortion first decreases and then increases, as shown in Fig. 2 (g), unlike in BaTiO_3 ³, where the imaginary frequen-

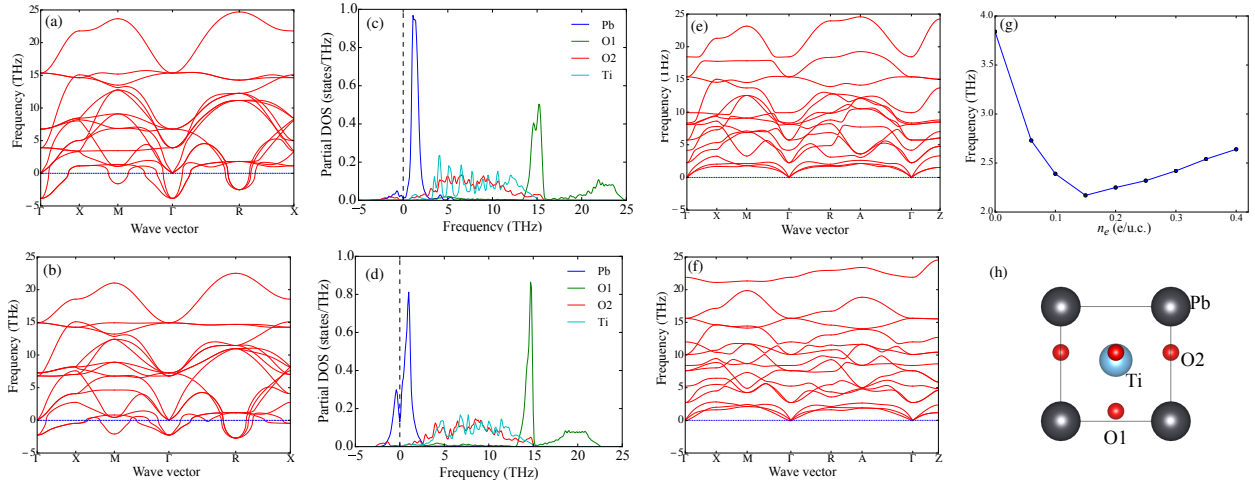


FIG. 2: The phonon band structures of the (a) $Pm\bar{3}m$ structure without doping, (b) $Pm\bar{3}m$ structure with electron doping ($n_e = 0.2$ e/u.c.), (c) $P4mm$ structure without doping, (f) $P4mm$ structure with electron doping ($n_e = 0.2$ e/u.c.). (c) and (d) are the atom projected partial phonon density of states projected on the [001] direction for the $Pm\bar{3}m$ structure without doping and with electron doping ($n_e = 0.2$ e/u.c.), respectively. The imaginary phonon frequencies are shown as negative numbers. The high symmetry q-vectors for $Pm\bar{3}m$ are Γ (0, 0, 0), X (0, 1/2, 0), M (1/2, 1/2, 0), R (1/2, 1/2, 1/2). The high symmetry q-vectors for $P4mm$ are Γ (0, 0, 0), X (0, 1/2, 0), M (1/2, 1/2, 0), R (0, 1/2, 1/2), A (1/2, 1/2, 1/2), Z (0, 0, 1/2). (g) The imaginary frequencies at Γ with electron doping. (h) is the $P4mm$ structure with polar distortion along the [001] direction.

cies disappear as the concentration of electrons increases. The atom projected phonon densities of states (PDOS) for $n_e=0$ and $n_e=0.2$ e/u.c. are shown in Fig. 2 (c) and (d), respectively. For both most $n_e=0$ and $n_e=0.2$ e/u.c., most of the PDOS in the imaginary frequency region is projected on the Pb sites, and a small portion is projected on the O sites in the side plane (O2 in Fig. 2 (h)), indicating that the soft phonons are from the Pb atoms and the O atoms in the side plane. The results consist with that the lone pair is from the Pb-O2 electron hybridization³⁴. From Figs. 2 (e) and (f), it can be seen that there are no imaginary frequencies in the phonon bands in the $P4mm$ phase, indicating the $P4mm$ phase being stable.

From Fig. 2, it can be seen that the soft phonons in the $Pm\bar{3}m$ phase due to the Pb ion and the O ions in the side plane do not disappear with the electron doping. Here we analyze the electronic structure of $PbTiO_3$ to show why: the coupling between the Pb-O bands and the doping of electrons is weak. The density of states is shown in Fig. 3 (a). As electrons are doped, the Fermi energy is pushed into the conduction band, which is mostly constitute by the Ti 3d states. Figure 3 shows that the Fermi energy is quite far away from the valence Pb and O bands, which means the shifting of Fermi energy does not strongly affect the occupation of the Pb and O bands. The lone pair, which is a hybrid of the Pb cation (s, p) and the nearest O anion p states, is the key factor for the polar distortion. We calculated the COHP of the Pb-O bond to see the change of the hybridization, as shown in Fig. 3 (b). It can be seen that the change of the Pb-O hybridization is small. The positive and negative values in the COHP indicate bonding and anti-bonding interaction between Pb and O orbitals, respectively. It can be seen that the energy range related to the lone pair (the anti-bonding Pb-O states at the top of the valence band³⁴) is far away from the energies of the doped electrons, thus the change

in the anti-bonding states corresponding to the lone pairs are small. The lone-pair states corresponding to the antibonding Pb-O states are characterized by the asymmetric ELF lobes around the Pb ions in the electron-doped structure as shown in Figs. 3 (c) and (d), which also shows that the Pb lone pairs are not destroyed by the doped electrons. The strong Pb-O hybridization leading to the lone pairs favor the short Pb-O bonds (marked in red in Fig. 3 (c)) and thus drive the Pb ions away from their central symmetric positions, resulting in the polar distortion.

The weak coupling between the Pb lone pair and the electron doping only ensure that the ferroelectric distortion persists. Then what is the reason for the enhancement of the ferroelectric distortion? Here we show that the enhancement of the polar distortion is related to the increasing of the volume of the structure. The volume of $PbTiO_3$ increases with the concentration of the doped electrons, as shown in Fig. 1 (c), because the doped electrons mainly stay on the Ti 3d orbitals, increasing the Ti ion radius.

We calculated the changes of the polar distortion of $PbTiO_3$ with negative hydrostatic pressure. The changes of the distortion with electron doping were plotted as functions of lattice volume and then compared to those with hydrostatic pressure, as shown in Fig. 4. The changes of c/a and cation-anion displacements with the same lattice volume are close in the two situations, indicating the the enhancement of the polar distortion with electron doping is related to the increasing of the lattice volume. It can be also seen that there is an anomalous enhancement of tetragonality and lattice volume as n_e increases to about 0.3 e/u.c. (Fig. 1), which was also found in $PbTiO_3$ with negative pressure³⁵. We examined the Pb-O bonds to see how the increasing of the volume affects the polar distortion. The lengths of the Pb-O bonds are plotted in Fig. 5. The 12

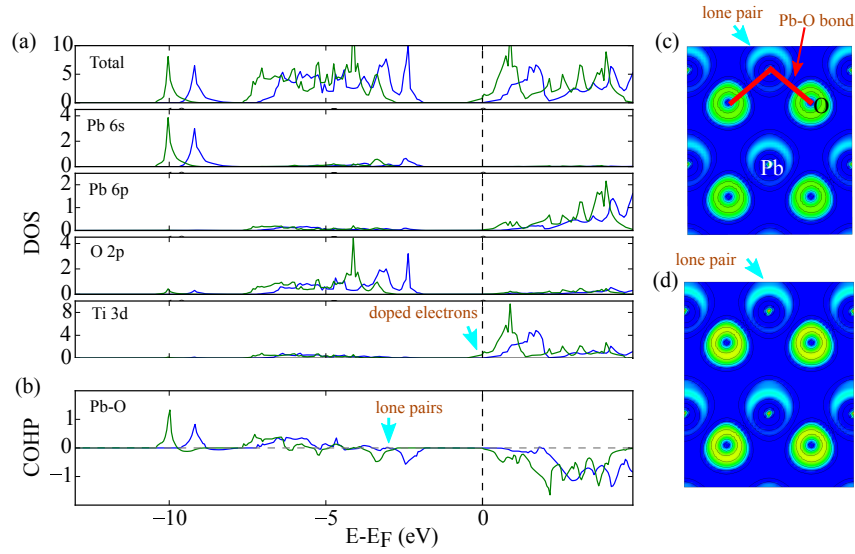


FIG. 3: (a) The density of states in PbTiO₃. (b) The COHP of the Pb-O bond. In (a) and (b), the blue lines and the green lines represent the results in the non-doped and doped PbTiO₃ structures, respectively. The results for non-doped structure are shifted so that the Fermi energy is at the conduction band minimum so that the DOSes for the doped and non-doped structures can be more easily compared. The concentration of the doped electrons is $n_e = 0.2$ e/u.c.. (c) and (d) are the contour maps of the ELFIs in the $a - c$ PbO plane of the doped and non-doped structures, respectively. The Pb-O bonds corresponding to the lone-pair indicated by the cyan arrow are marked in red in (c).

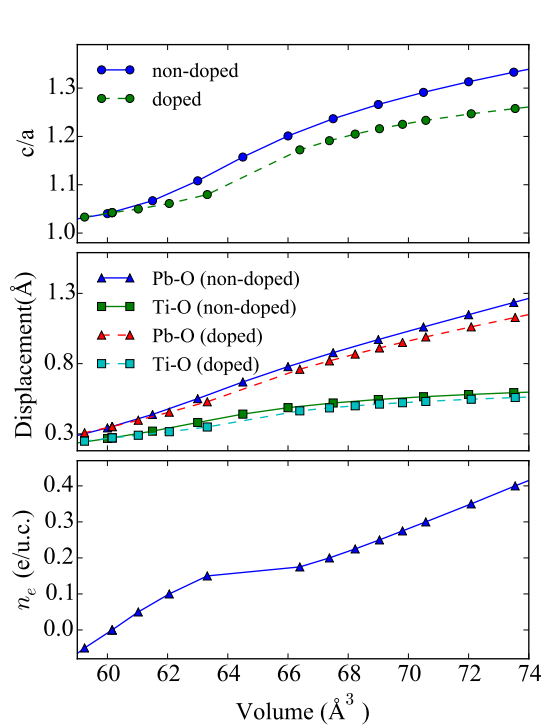


FIG. 4: (a) The ratio c/a as the function of lattice volume. (b) The relative displacements of Pb-O and Ti-O as functions of lattice volume. (c) The concentration of the doped electrons corresponding to the volume. The results for the non-doped structures were calculated by add negative hydrostatic pressure.

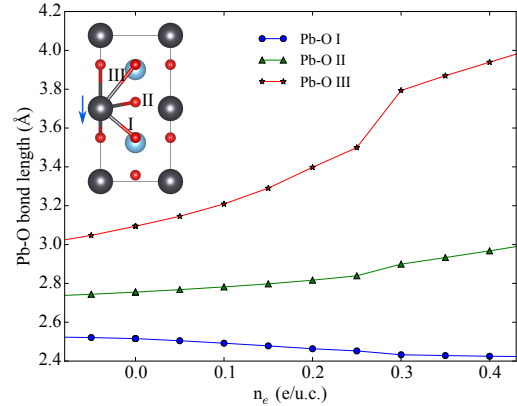


FIG. 5: The change of lengths the Pb-O bonds with the concentration of doped electrons. The 12 Pb-O bonds for each Pb ion are classified into 3 groups denoted as I, II, and III due to the 4 fold rotation symmetry in the $P4mm$ structure. The blue arrow shows the shift of the Pb ion with the increasing of n_e .

Pb-O bonds of each Pb ion can be classified into 3 groups (denoted as type I, II, and III in Fig. 5) because of the four fold rotation symmetry in the $P4mm$ structure. As the doped electrons enlarge the sizes of Ti ions, the Pb-O chain consisting of alternating type I and type III bonds are stretched. The changes of the type I bond lengths are relatively small, while those of the type III bond lengths are much larger. It can also be seen that the type I/III Pb-O bonds are much shorter/longer than the sum of the Shannon radius of Pb^{2+} ion (1.63\AA) and that of the O^{2-} ion (1.21\AA). The reason is that the hybridization between the Pb 6s states and the O 2p states stabilizes the short Pb-O

type I bonds and the forming or the lone pairs. Thus the type III bonds are elongated, leading to weaker attraction forces between the Pb and O ions in the type III bonds. Consequently, Pb ions displace towards the side of type I bonds, decreasing the lengths of the type I bonds. As the displacements of the Pb ions along the [001] direction increase, the angles (θ) between the type II bonds and the (001) plane are larger. The lengths of the type II bonds ($a/\cos\theta$) are thus increased. To compensate this elongation of the type II bonds, the in-plane lattice constant a reduces, leading to larger c/a .

There are some similarities between the electron doped PbTiO_3 and the NCSM LiOsO_3 . Firstly, the long range Coulomb interaction is screened out and is not a necessity for the lone-pair-driven polar structures. Secondly, in both structures, the polar distortions are due to the small A-site ions. (The ionic radius of Pb ion is small on one side due to the formation of the lone pair.) Thirdly, the Fermi energy is in the B-site bands and outside the energy range of the electronic states related to the A-O interaction. These similarities infer that the polar distortion and the metallicity can coexist if they are from different atoms.

The mechanism of the persistent or even the enhancement of the polar distortion in PbTiO_3 with electron doping presented in this paper should be transferable to other lone-pair-driven ferroelectric materials, like in PbVO_3 ³⁶, BiFeO_3 ³⁷, SnTiO_3 ³⁴, BiMnO_3 ³⁸. In these materials, anti-bonding states corresponding to the lone pairs are in the valence bands, which is below the Fermi energy if electrons are doped. Whereas the bottom of conduction bands in these materials are often the B-site states. Thus the doping of electrons can be seen as a selective enlargement of the B-site ion radius, which can increase the volume of the lattice and stretch the A-O bonds. Therefore, enhancement of polar distortion in these materials similar to that in PbTiO_3 is likely to emerge. These results also imply that the lone-pair stereoactive ions can be used as the A-site ions in perovskites to form NCSMs. By selecting a B-site

element (or elements) with suitable ionic radius and itinerant electrons, lone-pair-driven non-central-symmetric metal may be designed.

IV. CONCLUSION

In this work, we investigated the effect of electron doping on the lone-pair driven polar distortion by carrying out density functional theory studies on PbTiO_3 . We found that the polar distortion is enhanced with electron doping in PbTiO_3 . The long-range Coulomb interaction is screened out by the doped electrons, which indicates that the long-range Coulomb interaction is not necessary for the polar distortion. The analysis on the phonons and electronic states shows the mechanism for the persistent of the polar distortion: the forming of the electron lone pairs, which is the driving force of the polar distortion, is not affected much by the electron doping, because the energy range of the electron states related to the lone pairs is far enough from the Fermi energy. We also found that the enhancement of the polar distortion in PbTiO_3 is a combined effect of the lone pair and the increasing of the lattice volume caused by the electron doping. These results show that the lone-pair driven polar distortion and the metallicity can coexist, and it is highly expected that the lone-pair-stereoactive ions can be used in designing NCSMs.

ACKNOWLEDGMENTS

The work was supported by the National Basic Research Program of China (Nos. 2014CB921001 and 2012CB921403), the National Natural Science Foundation of China (No. 11134012), and the Strategic Priority Research Program (B) of the Chinese Academy of Sciences (No. XDB07030200).

-
- ¹ L. Liu, H. Guo, H. Lu, S. Dai, B. Cheng, and Z. Chen, *J. Appl. Phys.* **97**, 054102 (2005).
 - ² K. Page, T. Kolodiazny, T. Proffen, A. K. Cheetham, and R. Sehadri, *Phys. Rev. Lett.* **101**, 205502 (2008).
 - ³ Y. Wang, X. Liu, J. D. Burton, S. S. Jaswal, and E. Y. Tsymlal, *Phys. Rev. Lett.* **109**, 247601 (2012).
 - ⁴ Y. Iwazaki, T. Suzuki, Y. Mizuno, and S. Tsuneyuki, *Phys. Rev. B* **86**, 214103 (2012).
 - ⁵ P. W. Anderson and E. I. Blount, *Phys. Rev. Lett.* **14**, 217 (1965).
 - ⁶ D. Puggioni and J. M. Rondinelli, *Nat. Commun.* **5** (2014), 10.1038/ncomms4432.
 - ⁷ Y. Shi, Y. Guo, X. Wang, A. J. Princep, D. Khalyavin, P. Manuel, Y. Michiue, A. Sato, K. Tsuda, S. Yu, *et al.*, *Nat. Mater.* **12**, 1024 (2013).
 - ⁸ N. Benedek and T. Birol, *J. Mater. Chem. C*, (2016).
 - ⁹ H. Sim and B. G. Kim, *Phys. Rev. B* **89**, 201107 (2014).
 - ¹⁰ H. J. Xiang, *Phys. Rev. B* **90**, 094108 (2014).
 - ¹¹ G. Giovannetti and M. Capone, *Phys. Rev. B* **90**, 195113 (2014).
 - ¹² H. M. Liu, Y. P. Du, Y. L. Xie, J.-M. Liu, C.-G. Duan, and X. Wan, *Phys. Rev. B* **91**, 064104 (2015).
 - ¹³ V. P. Mineev and Y. Yoshioka, *Phys. Rev. B* **81**, 094525 (2010).
 - ¹⁴ V. M. Edelstein, *Phys. Rev. B* **83**, 113109 (2011).
 - ¹⁵ V. M. Edelstein, *Phys. Rev. Lett.* **75**, 2004 (1995).
 - ¹⁶ V. M. Edelstein, *J. Phys.: Condens. Matter* **8**, 339 (1996).
 - ¹⁷ G. Kresse and D. Joubert, *Phys. Rev. B* **59**, 1758 (1999).
 - ¹⁸ G. Kresse and J. Furthmüller, *Phys. Rev. B* **54**, 11169 (1996).
 - ¹⁹ J. P. Perdew and A. Zunger, *Phys. Rev. B* **23**, 5048 (1981).
 - ²⁰ G. Shirane, R. Pepinsky, and B. C. Frazer, *Acta Crystallogr.* **9**, 131 (1956).
 - ²¹ G. Sághi-Szabó, R. E. Cohen, and H. Krakauer, *Phys. Rev. Lett.* **80**, 4321 (1998).
 - ²² G. Makov and M. C. Payne, *Phys. Rev. B* **51**, 4014 (1995).
 - ²³ S. Lany and A. Zunger, *Phys. Rev. B* **78**, 235104 (2008).
 - ²⁴ S. Baroni, S. de Gironcoli, A. Dal Corso, and P. Giannozzi, *Rev. Mod. Phys.* **73**, 515 (2001).
 - ²⁵ A. Togo and I. Tanaka, *Scr. Mater.* **108**, 1 (2015).
 - ²⁶ R. Dronskowski and P. E. Bloechl, *J. Phys. Chem* **97**, 8617 (1993).
 - ²⁷ V. L. Deringer, A. L. TchougrAlef, and R. Dronskowski, *J. Phys. Chem. A* **115**, 5461 (2011), pMID: 21548594.

- ²⁸ S. Maintz, V. L. Deringer, A. L. TchougrÃeff, and R. Dronskowski, *J. Comput. Chem.* **34**, 2557 (2013).
- ²⁹ J. Ãniguez, D. Vanderbilt, and L. Bellaiche, *Phys. Rev. B* **67**, 224107 (2003).
- ³⁰ K. Momma and F. Izumi, *J. Appl. Crystallogr.* **41**, 653 (2008).
- ³¹ X. Wu, D. Vanderbilt, and D. R. Hamann, *Phys. Rev. B* **72**, 035105 (2005).
- ³² H. Moriwake, C. A. J. Fisher, A. Kuwabara, and T. Hashimoto, *Japanese Journal of Applied Physics* **50**, 09NE02 (2011).
- ³³ R. D. Shannon, *Acta Crystallographica Section A* **32**, 751 (1976).
- ³⁴ K. C. Pitike, W. D. Parker, L. Louis, and S. M. Nakhmanson, *Phys. Rev. B* **91**, 035112 (2015).
- ³⁵ S. Tinte, K. M. Rabe, and D. Vanderbilt, *Phys. Rev. B* **68**, 144105 (2003).
- ³⁶ D. J. Singh, *Phys. Rev. B* **73**, 094102 (2006).
- ³⁷ P. Ravindran, R. Vidya, A. Kjekshus, H. Fjellvåg, and O. Eriksson, *Phys. Rev. B* **74**, 224412 (2006).
- ³⁸ R. Seshadri and N. A. Hill, *Chem. Mater.* **13**, 2892 (2001).